Stimulation of non-classical receptive field enhances orientation selectivity in the cat

Gang Chen[1,3], Yang Dan[2] and Chao-Yi Li[1]

[1] *Institute of Neuroscience, Shanghai Institutes of Biological Sciences, Chinese Academy of Sciences, Shanghai 200031, China*
[2] *Department of Molecular and Cell Biology, University of California, Berkeley, CA 94720, USA*
[3] *Graduate School of the Chinese Academy of Sciences, Beijing 100037, China*

We have investigated how the nonclassical receptive field (nCRF) affects dynamic orientation selectivity of cells in the primary visual cortex (V1) in anaesthetized and paralysed cats using the reverse correlation method. We found that tuning to the orientation of the test stimulus depends on the size of the stimulation area. A significant sharpening of orientation tuning was induced by nCRF stimulation, with the magnitude of the effect increasing with the size of stimulation. The effect of the nCRF on the temporal dynamics of orientation tuning was also investigated by examining the tuning over a range of delays from stimulus onset. We found small but detectable changes in both the preferred orientation and the bandwidth of tuning over time when the classical receptive field (CRF) was stimulated alone. Stimulation in nCRF significantly increased the magnitude of these temporal changes. Thus, nCRF stimulation not only enhances the overall orientation selectivity, but also enriches the temporal dynamics of cortical neurones, which may increase the computational power of the visual cortex in information processing.

(Resubmitted 25 November 2004; accepted after revision 24 January 2005; first published online 27 January 2005)
Corresponding author C.-Y. Li: Institute of Neuroscience, Shanghai Institutes of Biological Sciences, Chinese Academy of Sciences, Shanghai 200031, China. Email: cyli@sibs.ac.cn

Orientation selectivity is an important emergent property of neurones in the primary visual cortex (V1). Traditionally, orientation tuning is estimated by measuring the firing rate of the neurone evoked by orientated gratings or bars, and the response at each orientation is averaged over seconds. This approach can yield an accurate estimate of orientation selectivity, but it does not reveal the temporal development of the selectivity, which may provide important clues about the underlying circuitry. An alternative method is to measure the responses to rapidly flashed gratings at a random sequence of orientations, and to use reverse correlation to analyse the temporal dynamics of orientation tuning (Ringach *et al.* 1997*a*; Dragoi *et al.* 2002; Felsen *et al.* 2002; Mazer *et al.* 2002). Using this method, a recent study in anaesthetized monkey has shown that both the bandwidth and the peak of orientation tuning may change over time (Ringach *et al.* 2003). Other groups, however, did not find substantial evidence for dynamic changes in orientation tuning (Gillespie *et al.* 2001; Mazer *et al.* 2002). In this study, we measured the dynamics of orientation tuning with a similar method, and found evidence for the temporal changes in the tuning property.

Furthermore, we varied the area covered by the grating stimuli to explore the effects of the nonclassical receptive field (nCRF) stimulation on orientation selectivity and dynamics. Visual stimulation in the nCRF is known to strongly modulate the responses to classical receptive field (CRF) stimulation (Allman *et al.* 1985; Fitzpatrick, 2000), and the functional properties of nCRF have been widely investigated in both the cat (Blakemore & Tobin, 1972; Maffei & Fiorentini, 1976; DeAngelis *et al.* 1994; Li & Li, 1994; Sengpiel *et al.* 1997; Polat *et al.* 1998; Bringuier *et al.* 1999; Anderson *et al.* 2001; Ozeki *et al.* 2004) and the monkey (Levitt & Lund, 1997; Kapadia *et al.* 1999; Sceniak *et al.* 1999; Jones *et al.* 2001; Rossi *et al.* 2001; Cavanaugh *et al.* 2002*a*). Many investigators suggested that nCRF may be involved in figure-ground segmentation and perceptual pop-out (Knierim & van Essen, 1992; Lamme, 1995; Walker *et al.* 1999; Akasaki *et al.* 2002; Jones *et al.* 2002). Others argued that nCRF increases the efficiency of information transfer, and plays an important role in sparse coding (Vinje & Gallant, 2000, 2002; Muller *et al.* 2003). According to the latter hypothesis, the nCRF is expected to enhance the selectivity of the cell. In this study, we investigated the effect of nCRF on orientation selectivity of V1 cells. We found that nCRF stimulation significantly sharpens orientation tuning and affects its temporal dynamics at all cortical layers for both simple and complex cells.

DOI: 10.1113/jphysiol.2004.080051

Methods

Electrophysiology

Acute experiments were performed on adult cats. All procedures complied with the guidelines laid by the Animal Research Advisory Committee at the Shanghai Institutes of Biological Sciences, Chinese Academy of Sciences. Detailed descriptions of procedures for animal surgery, anaesthesia and recording technique are available in Li & Li (1994). Briefly, cats were anaesthetized prior to surgery with ketamine hydrochloride (30 mg kg^{-1}, I.M.), and then tracheal and venous cannulations were carried out. After the operation, the animal was placed in a stereotaxic frame for craniotomy and subsequent visual experiments. Further surgery was performed under urethane (20 mg kg^{-1} h^{-1}, I.V.) anaesthesia. A craniotomy (2 mm diameter) was performed at the recording site in the striate cortex, and the dura was removed. The neuromuscular block (gallamine triethiodide, 10 mg kg^{-1} h^{-1}, I.V.) was applied to minimize the influence of eye movements about 1.5 h after all surgery had been completed, and at least 2 h after the anaesthetic was changed to urethane. Lidocaine (lignocaine) was applied to all wound margins and pressure points. During recording, anaesthesia and paralysis were maintained with gallamine triethiodide (10 mg kg^{-1} h^{-1}), urethane (20 mg kg^{-1} h^{-1}) and glucose (200 mg kg^{-1} h^{-1}) in Ringer solution (3 ml kg^{-1} h^{-1}). End-expiratory CO_2 was kept at 4%, and core body temperature at 38°C. Electroencephalogram and ECG were monitored continuously. Anaesthesia was considered sufficient when EEG was in a permanent sleep-like state. Several reflexes, including corneal, eyelid and withdrawal reflexes, were tested every 15 min during the surgery. After the neuromuscular block had been applied, a toe-pinch test, in which one of the toes of the animal was pressed with a force which might elicit an avoidance response in the conscious one, was used to estimate the anaesthesia status every 2 h. If the heart rate increased more than 20% in 1 min after the test, additional urethane I.V. was given immediately, and the drip rate was increased. The toe-pinch test was repeated every 10 min until no positive response was found within 1 h. The nictitating membranes were retracted and pupils dilated. Artificial pupils of 3 mm diameter were used. Contact lenses and additional corrective lenses were applied to focus the retina onto a screen. Single-unit recordings were made in the V1 using tungsten-in-glass microelectrodes (Li *et al.* 1995). Recorded signals were amplified, filtered and discriminated with a hardware window discriminator. Detected action potentials were time stamped with an accuracy of 1 ms. Only well-isolated cells satisfying strict criteria for single-unit recording (fixed shape of the action potential, absence of spikes during the absolute refractory period) were included for further analyses. At the end of data collection, the animal was killed by an overdose of barbiturate I.V.

Visual stimuli

Custom software run on a computer with a high-resolution graphics board was used to generate visual stimuli in real time. Images were presented on a monitor at 100 Hz vertical refresh rate, with a mean luminance of 20 cd m^{-2}. Luminance nonlinearities were corrected through the software. The monitor was placed 57 cm from the eyes. For each cell isolated, the centre of CRF was first located with a manually controlled grating patch with a contrast of 40%. Then, orientation, spatial frequency and temporal frequency of the patch were systematically optimized with computer control during stimulation to the dominant eye. We employed the reverse correlation method to obtain the orientation selectivity of the cell (Ringach *et al.* 1997*a*,*b*, 2003; Dragoi *et al.* 2002; Felsen *et al.* 2002; Mazer *et al.* 2002; Yao *et al.* 2004). The stimulus sequence used in our experiment consisted of 57 600 preset patterns, with each stimulus pattern lasting for two frames (corresponding to an effective frame rate of 50 Hz, for a duration of 20 min). Each frame contained a sinusoidal grating (100% contrast) presented at the optimal spatial frequency for each cell over CRF. The orientation and the spatial phase of the gratings at each frame were selected randomly from a stimulus pool which contained 12 predetermined orientations evenly distributed between 0 and 165 deg, and eight spatial phases (0, ±45, ±90, ±135 and ±180 deg, the centre of the stimulated area was defined as 0 deg). The stimulus size was chosen to be 1×, 2× and 4× the size of CRF for each cell (the rest of the screen was blank, at 20 cd m^{-2}). In the first set of experiments, we measured the orientation selectivity using a sequence with constant stimulus size (Fig. 1*A*); the size varied in different sequences. In the second set of experiments, we measured the responses using a sequence containing multiple stimulus sizes, ranging from 1 × CRF to 5.5 × CRF (Fig. 1*B*).

Histological reconstruction of the electrode tracks

At the end of some penetrations, an electrolytic lesion was made by passing a current (10 μA for 10 s) through the tip of the electrode; then the electrode was withdrawn and two more lesions were made (Yao & Li, 2002). At the end of the experiment, the animal was given an overdose of barbiturate, and was perfused transcardially with 10% formaldehyde in 0.9% saline. The fixed brain was cut into blocks and sectioned to 100 μm thickness. Electrode tracks were reconstructed from the sections stained with cresyl violet. The locations of the electrodes were confirmed to be within area 17, which has a thicker layer IV than the neighbouring area 18 (O'Leary, 1941; Orban, 1984), and cortical laminae were identified by the criteria of Gilbert (1977) and Lund *et al.* (1979).

Data analysis

Only cells whose circular variance (defined as

$$V = 1 - \frac{|\sum_k R_k e^{(i\,2\theta_k)}|}{\sum_k R_k}$$

where R_k is the response at orientation $\theta_k < 0\,\text{deg} < 180\,\text{deg}$) is less than 0.9 were included (Worgotter & Eysel, 1987; Leventhal *et al.* 1995). Among the 168 cells tested with the stimuli in Fig 1*A*, 30 simple and 96 complex cells fit this criterion at all three latencies (T_{dev}, T_{opt} and T_{dec}, see below), which were used for further analysis. For the 43 cells tested with the stimuli in Fig 1*B*, 31 cells fit the criterion at all stimulus sizes, and were used in the analysis.

Basic characterization. Cells were classified as simple or complex according to the relative modulation in the responses to drifting sinusoidal gratings (the ratio of the first harmonic to the mean firing rate, after subtracting the average spontaneous rate) (Skottun *et al.* 1991). We estimated the size of the CRF using an occlusion test in which blank circular apertures (at the mean luminance, 20 cd m^{-2}) with different diameters were presented on the background of a full field grating to concentrically occlude CRF (Li & Li, 1994; Yao & Li, 2002). The minimum mask diameter at which the responses were reduced to the spontaneous level was defined as the size of CRF. The nCRF properties of the neurone were assessed by comparing the neuronal response to dynamic grating at the size of 1 × CRF with that at 4 × CRF. About half of cells (68/126) had inhibitory nCRF (response at 4 × CRF significantly smaller than that at 1 × CRF), 16/126 cells showed no significant difference between the responses at 1 × CRF and 4 × CRF, and 42/126 cells had facilitatory nCRF.

Temporal-orientation matrix (TOM). Reverse correlation method in the orientation domain was used to measure the time evolution of orientation tuning. In order to analyse the data of the first set of experiments (Fig. 1*A*), we constructed a temporal-orientation matrix (TOM), which represents the firing rate of the neurone at t (milliseconds) following the presentation of each orientation (averaged across all occurrences of the orientation at all phases). Stimulus size was constant throughout each stimulus sequence, and different TOMs were computed from the responses measured at different stimulus sizes, ranging from 1 × CRF to 4 × CRF. For the data in the second set of experiments (Fig. 1*B*), the main analysis procedures were the same as in the first set of experiments, except that TOMs were expanded to a three-dimensional matrix, varying in orientation, response latency and stimulus size.

Optimal latency. In order to estimate the temporal response of the cell, we defined a response variance index as the standard deviation of the responses to different orientations (R_{Ori}) at each latency T (Fig. 2*B*):

$$V(T) = \left\{ \frac{1}{n} \sum_{\text{Ori}=1}^{n} \left[R_{\text{Ori}}(T) - \frac{1}{n} \sum_{\text{Ori}=1}^{n} R_{\text{Ori}}(T) \right]^2 \right\}^{\frac{1}{2}} \quad (1)$$

Optimal latency (T_{opt}) of the neural response was defined as the peak of the Gaussian fit:

$$V(T) = V_0 + V_1 e^{\frac{-(T-T_{\text{opt}})^2}{\sigma_T^2}}$$

where V_0, V_1, T_{opt}, and σ_T are free parameters), indicated by the vertical dashed lines in Fig. 2*A* and *B*. The fitted curve was not constrained to pass through the overall peak response point, although in practice T_{opt} is very close to this point.

Tuning width. The orientation tuning curves were fitted with the von Mises distribution:

$$R = R_0 + R_1 e^{k\left[\cos 2(\text{Ori}-\text{Ori}_p)-1\right]} \quad (2)$$

where R represents the response of the cell as a function of orientation (Ori), and R_1, R_0, Ori_p and k are free parameters (Swindale, 1998). Fitting was made to the raw data rather than the mean response at each orientation. The preferred orientation was defined as the peak of the fitted function (Ori_p). Width at half-height (WHH) of the fitted function was used to describe the tuning width,

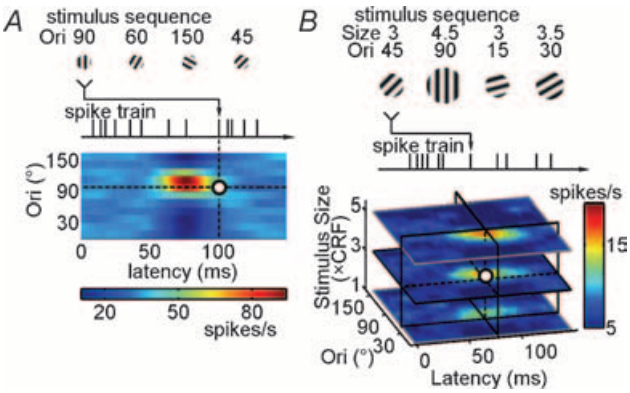

Figure 1. Reverse correlation method for analysing the cortical responses to dynamic grating stimuli
A, dynamic grating stimuli (at a fixed stimulus size), cortical spike train, and the temporal-orientation matrix (TOM) representing the response of a V1 neurone as a function of both stimulus orientation and latency (colour scale shown below). *B*, dynamic grating stimuli in which both orientation and size of the grating varied in a pseudorandom sequence, and the tuning of the cell is represented by a three-dimensional matrix, in which the response is a function of orientation, latency and stimulus size.

which was calculated as follows:

$$\mathrm{WHH} = \arccos\left[(\ln 0.5 + k)/k\right] \quad (3)$$

Goodness of fit. This was measured by χ_N^2:

$$\chi_N^2 = \frac{1}{N}\sum_n \frac{(R_n - F_n)^2}{\sigma_n^2} \quad (4)$$

where N is the number of degrees of freedom, R_n is the response to the nth stimulus, F_n is the prediction based on the von Mises distribution, and σ is the variance of R_n (Sengpiel *et al.* 1998; Swindale, 1998; Cavanaugh *et al.* 2002*a*). All cells with P values (determined by χ_N^2) in the range of 0.1–1 were included for further analysis (Swindale, 1998).

The sharpening effect induced by the nCRF was measured by the sharpening index as:

$$\mathrm{Index}_{\mathrm{sharpen}} = \frac{\mathrm{WHH}_{\mathrm{CRF}} - \mathrm{WHH}_{n\mathrm{CRF}}}{\mathrm{WHH}_{\mathrm{CRF}}} \quad (5)$$

Changes in tuning over time. The tuning widths at two latencies, 10 ms before (development phase, T_{dev}) and 10 ms after (decay phase, T_{dec}) T_{opt}, were selected to measure the changes of tuning over time. These latencies were chosen because at these points the peak and width of orientation tuning could still be measured with reasonable accuracy, and the interval between the two points (20 ms) allowed detectable evolution of the tuning curve. At longer intervals (e.g. 20 ms before and after T_{opt}), the amplitudes and hence the signal-to-noise ratios of the measured tuning curves were considerably lower, thus it was difficult to obtain a reliable measure of the tuning peak and width.

Inseparability. An important measure of the temporal dynamics of orientation tuning used in this study is the orientation–time inseparability, which was computed with singular value decomposition (SVD). The TOM was transformed into the linear sum of n separable matrixes (Golub & Van Loan, 1996) as:

$$\mathrm{TOM}(i,\, j) = U\Lambda V^T + M = \sum_{i=1}^{n} \lambda_i u_i v_i^T + M;$$
$$\Lambda = \mathrm{diag}(\lambda_1, \lambda_2, \ldots \lambda_n), \quad \lambda_1 \geq \lambda_2 \geq \cdots \geq \lambda_n \quad (6)$$

U and V are the singular vectors, Λ is a diagonal matrix of singular values, and M is the mean response of the cell. The more separable the TOM is, the more precisely the matrix can be reconstructed by the first singular vector. The inseparability index was measured by the relative weight of the first singular value (Depireux *et al.* 2001; Pena & Konishi, 2001; Mazer *et al.* 2002) as:

$$\mathrm{Index}_{\mathrm{inseparability}} = \left(1 - \lambda_1^2 \Big/ \sum_{i=1}^{n} \lambda_i^2\right) \times 100 \quad (7)$$

The value of this index ranged from 0 to 100 (in unit of percentage). Values approaching zero indicate that only the first singular value is nonzero, and a larger value suggests a higher level of inseparability.

Data are presented as means ± S.E.M., and statistical significance was determined by Student's t test. For individual cells, confidence intervals for the estimated parameters were determined by the bootstrap method (Manly, 1997). A total of 1000 simulations were performed to determine 95% confidence intervals for each parameter.

Results

Single-unit recordings were made in the V1 of the anaesthetized adult cat. A total of 30 simple cells and 96 complex cells were recorded.

Effect of nCRF stimulation on response latency

We measured the neuronal responses to dynamic grating stimuli and used the reverse correlation method to compute orientation tuning at different response latencies (Fig. 1*A*), which was referred to as the TOM. We first tested whether nCRF stimulation affects the time course of the neuronal responses. Based on the TOM of each cell (Fig. 2*A*), we computed the variance index as a function of

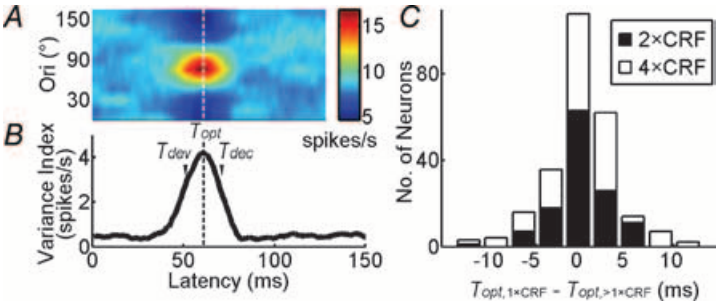

Figure 2. Stimulus size does not affect the optimal latency
A, TOM of an example cell. *B*, index of variance as a function of response latency. The vertical dashed line indicates optimal latency (T_{opt}), defined as the peak position of the Gaussian fit. T_{dev} and T_{dec} are defined as 10 ms before and after T_{opt}, respectively. *C*, distribution of the difference between T_{opt} at 1 × classical receptive field (CRF) and >1 × CRF ($n = 126$). The mean of the difference was not significantly different from 0 ($P > 0.4$ and $P > 0.2$ for 2 × CRF and 4 × CRF, respectively, paired t test).

response delay (Fig. 2*B*) to determine the optimal latency (T_{opt}, vertical dashed line; see Methods). We found that the optimal latencies at different stimulus sizes were similar (Fig. 2*C*). The mean optimal latencies were 62.3 ± 1.0 ms ($n = 126$), 62.1 ± 1.1 ms, and 61.9 ± 1.1 ms for stimulus sizes of 1×, 2× and 4 × CRF, respectively; no significant difference was found among different sizes ($P = 0.96$, ANOVA). Thus, nCRF stimulation does not affect the response latency, and the optimal latency obtained at 1 × CRF was used for further analyses.

nCRF stimulation sharpens orientation tuning

We next tested whether nCRF stimulation affects orientation tuning at T_{opt} by comparing the tuning curves at different sizes. Each curve was fitted with von Mises distribution, and the tuning width is defined as the WHH of the fit (see Methods). Figure 3*A* shows the results for two cells. For the cell on the left, the widths of orientation tuning (horizontal arrows) were 56.0, 40.4 and 33.7 deg for stimulus sizes of 1×, 2× and 4 × CRF, respectively; $\text{Index}_{\text{sharpen}}$, which indicates the decrease in tuning width relative to that at 1 × CRF, was 27.9% at 2×, and 39.8% at 4 × CRF. For the cell on the right, the tuning widths were 48.6, 39.8 and 35.4 deg at 1×, 2× and 4 × CRF, respectively, exhibiting a similar sharpening effect induced by nCRF stimulation. Figure 3*B* shows a summary of the nCRF effect for the 126 cells studied. Most of the data points fell below the diagonal line, indicating that the orientation tuning was sharpened by nCRF stimulation. While the average tuning width at 1 × CRF was $59.3 \pm 2.6^{\circ}$, the widths at 2× and 4×CRF were 49.2 ± 2.2 and 44.8 ± 2.0, respectively, both of which were significantly narrower than that at 1 × CRF ($P < 10^{-6}$ and $P < 10^{-10}$, paired *t* test) (Fig. 3*C*). The extent of sharpening was found to be similar across cortical layers and for neurones with or without inhibitory nCRF (see Fig. 3 legend). To further characterize the relationship between the stimulus size and orientation selectivity, we measured the neuronal responses to dynamic grating stimuli that varied in both the orientation of the grating and the size of the stimulation area (Fig. 1*B*), which allowed us to map the orientation tuning at multiple sizes simultaneously. Figure 4*A* and *B* shows the tuning curves of an example cell at T_{opt} at different stimulus sizes. The tuning width narrowed systematically with the size, and its value at the largest stimulus size (5.5 × CRF) was 62.8% of that at 1 × CRF. Figure 4*C* shows $\text{Index}_{\text{sharpen}}$ as a function of stimulus size averaged over 31 cells. The slope of the robust fit curve for these data was significantly different from zero ($P < 10^{-9}$, robust regression), and the Pearson correlation coefficient between the relative tuning width and the stimulus size was 0.68. This result, which is similar to that shown in Fig. 3, further indicates that stimulation at larger sizes significantly sharpens the orientation tuning of the cell, which is consistent with finding in a previous study (Li & Li, 1994).

nCRF stimulation affects temporal dynamics of orientation tuning

Since nCRF is believed to be mediated by intracortical connections or feedback from higher areas (Lamme & Roelfsema, 2000; Angelucci & Bullier, 2003), the effect of nCRF stimulation may have a different time course from that of the feedforward input. We thus examined variations in the bandwidth of orientation tuning at

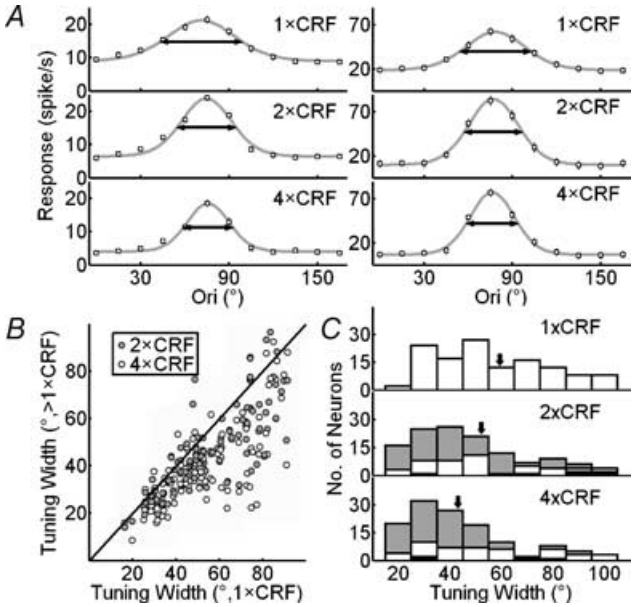

Figure 3. Bandwidth of orientation tuning decreases with nonclassical receptive field (nCRF) stimulation
A, orientation tuning curves extracted from TOM at T_{opt}, measured at 1×, 2× and 4 × CRF for two example cells. Lines indicate curve fitting with von Mises distribution. Horizontal arrows indicate widths at half-height (WHH) of the fits. Error bar, ±S.E.M. (for some points the error bars are smaller than the symbol). *B*, population summary of sharpening of orientation selectivity induced by nCRF stimulation. WHH obtained at 1 × CRF was plotted against those at >1 × CRF (2 × CRF and 4 × CRF). *C*, distributions of WHH at 1×, 2× and 4 × CRF. Arrows indicate means (59.3, 49.2 and 44.8 deg for 1×, 2× and 4 × CRF). Values for extent of sharpening relative to 1 × CRF were 13.6 ± 2.7 and 20.5 ± 2.7% for 2× and 4 × CRF, respectively, and were similar across all cortical layers (layer 2/3: 17.9 ± 2.6 and 24.3 ± 3.0% for 2× and 4 × CRF, respectively, $n = 44$; layer 4: 14.5 ± 3.6 and 22.9 ± 5.5%, $n = 14$; layer 5/6: 19.4 ± 3.5 and 25.7 ± 4.5%, $n = 33$), between simple and complex cells (simple cells: 11.9 ± 4.1 and 15.1 ± 4.3% for 2× and 4 × CRF, respectively, $n = 30$; complex cells: 14.2 ± 3.3 and 22.2 ± 3.2%, $n = 96$), and between cells with or without inhibitory nCRF (inhibitory at 2× and 4 × CRF: 13.6 ± 4.3 and 20.4 ± 4.0%, respectively, $n = 68$; facilitatory: 16.7 ± 3.7 and 22.3 ± 4.5%, $n = 42$; neither facilitatory nor inhibitory: 6.0 ± 5.7 and 16.3 ± 4.1%, $n = 16$). Grey: $\text{WHH}_{\text{CRF}} - \text{WHH}_{\text{nCRF}}$ significantly > 0; black: $\text{WHH}_{\text{CRF}} - \text{WHH}_{\text{nCRF}}$ significantly < 0. Significant sharpening occurred in 78 and 79 cells at 2 × CRF and 4 × CRF, and significant broadening occurred in 6 and 3 cells.

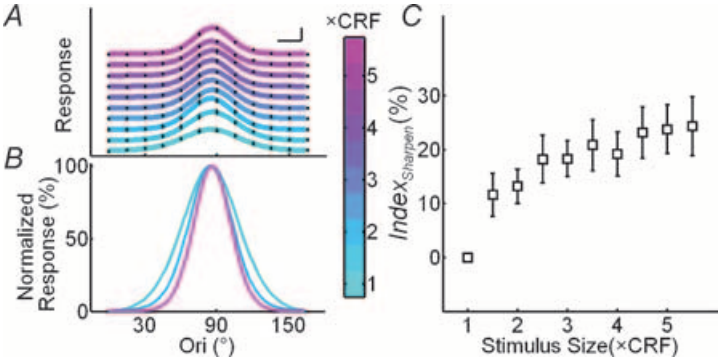

Figure 4. Orientation selectivity increases with stimulus size
In these experiments orientation tuning at multiple sizes was measured simultaneously (see Fig. 1*B*). *A*, orientation tuning curves at various stimulus sizes (colour indicates stimulus size, scale shown below). For clarity these curves were plotted with different vertical offsets. Filled circles, raw data; lines, curve fitting with von Mises distribution. Scale bars, 10 spikes s^{-1} and 20 deg. *B*, tuning curves at 1×, 3× and 5 × CRF, normalized by the peak of each curve to facilitate comparison of the tuning width. *C*, $\text{Index}_{\text{sharpen}}$ (defined as decrease in tuning width relative to that at 1 × CRF) as a function of stimulus size, averaged over 31 cells. Error bar, ±S.E.M.

different response latencies. In addition to the optimal delay (T_{opt}), we also measured the orientation tuning widths at 10 ms before (T_{dev}) and 10 ms after (T_{dec})T_{opt} and computed the difference between these two widths:

$$\Delta w = \frac{\text{WHH}_{T_{\text{dev}}} - \text{WHH}_{T_{\text{dec}}}}{\text{WHH}_{T_{\text{dev}}}}$$

Orientation tuning curves of an example cell at T_{dev} and T_{dec} obtained at 1 × CRF and 4 × CRF are shown in Fig. 5*A* and *B*, respectively. A decrease in the tuning

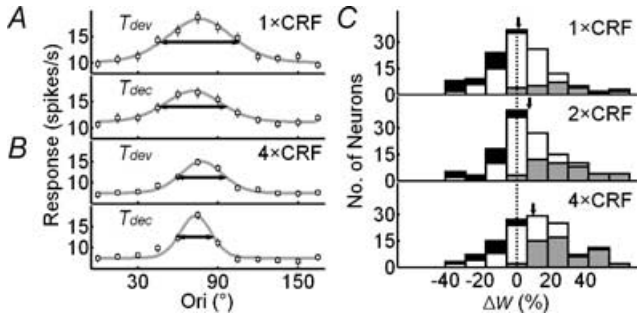

Figure 5. Stimulation of nCRF increases the temporal change in tuning width
A, tuning curves of a cell at T_{dev} and T_{dec} at 1 × CRF. *B*, tuning curves of the same cell at 4 × CRF. Filled circles, raw data; lines, curve fitting with von Mises distribution; horizontal arrows, WHH. The difference between WHH values at T_{dev} and T_{dec} was 14.8% at 1 × CRF and 27.0% at 4 × CRF. *C*, distributions of $\Delta w(\Delta w = \frac{\text{WHH}_{T_{\text{dev}}} - \text{WHH}_{T_{\text{dec}}}}{\text{WHH}_{T_{\text{dev}}}})$ for 126 cells at 1×, 2× and 4 × CRF. Arrows indicate means. Dashed vertical line, $\Delta w = 0$. Stimulus-size-dependent sharpening over time was found across all cortical layers (layer 2/3: 0.8 ± 3.0, 3.5 ± 2.5 and 8.7 ± 2.8% for 1×, 2× and 4 × CRF, respectively, $n = 44$; layer 4: 2.3 ± 3.9, 11.8 ± 5.2 and 8.7 ± 7.2, $n = 14$; layer 5/6: −3.8 ± 4.3, 6.1 ± 3.9 and 9.8 ± 4.3%, $n = 33$), for both simple and complex cells (simple cells: −0.2 ± 3.7, 4.2 ± 3.7 and 6.4 ± 4.9% for 1×, 2× and 4 × CRF, respectively, $n = 30$; complex cells: 1.1 ± 2.5, 8.0 ± 2.5 and 10.3 ± 2.6%, $n = 96$), and for cells with or without inhibitory nCRF (inhibitory: −0.6 ± 2.7, 7.2 ± 2.7 and 11.7 ± 2.4% for 1×, 2× and 4 × CRF, respectively, $n = 68$; facilitatory: 2.0 ± 3.6, 7.7 ± 4.3 and 6.6 ± 5.4%, $n = 42$; neither facilitatory nor inhibitory: 3.6 ± 7.4, 5.7 ± 2.7 and 7.2 ± 3.9%, $n = 16$). Neurones in which WHH significantly decreases over time are shown in grey, whereas the neurones with significant increase are shown in black. Significant decreases occur in 23, 41 and 52 cells, and significant increases occur in 20, 17 and 14 cells for stimulus sizes of 1×, 2× and 4 × CRF.

width over time was found under both conditions, with Δw being 14.8 and 27.0% at 1 × CRF and 4 × CRF, respectively. Figure 5*C* shows the distributions of Δw at 1×, 2× and 4 × CRF, with means of 0.8 ± 2.1, 7.1 ± 2.1 and 9.4 ± 2.3%, respectively. While Δw at 1 × CRF was not significantly different from 0 ($n = 126$, $P > 0.6$), it was significant with nCRF stimulation ($P < 0.001$ for 2 × CRF, and $P < 10^{-4}$ for 4 × CRF). A two-way ANOVA test showed that Δw depends significantly on stimulus size ($P = 0.02$), but not significantly on the laminar location of the cell ($P > 0.6$). Neurones with or without inhibitory nCRF showed similar Δw at all stimulus sizes ($P > 0.7$, $P > 0.9$ and $P > 0.5$ for 1 × CRF, 2 × CRF, and 4 × CRF). These results show that, while the changes are relatively small when only CRF is stimulated, the orientation tuning of cortical cells generally sharpens during the time course of the response when nCRF is stimulated.

In addition to the temporal changes in tuning width, we also analysed changes in the preferred orientation over time at various stimulus sizes. Figure 6*A* and *B* show the shift in the preferred orientation of a cell at 1 × CRF and 4 × CRF, respectively. At both stimulation sizes, the peak of the tuning curve shifted rightward over time (indicated by the arrows). In general, the high response variability of cortical cells makes it difficult to demonstrate the statistical significance of the changes. However, we found that the shift of the preferred orientation over time was correlated between different stimulus sizes (Pearson correlation coefficient was 0.78 between 1× and 2 × CRF and 0.74 between 1× and 4 × CRF, $n = 126$), indicating that the shifts were not due to random response variability. The slopes of the regression lines in Fig 6*C* and *D* were 0.69 and 0.46, respectively, which were significantly smaller than 1 (both $P < 0.001$), indicating that nCRF stimulation increased the shift in the preferred orientation. The shifts at 2 × CRF and 4 × CRF were also correlated (Pearson correlation coefficient was 0.81, Fig. 6*E*), and the slope of the regression line was 0.68, which was significantly smaller than 1 ($P < 0.001$), indicating that the effect at 4 × CRF is larger than that at 2 × CRF.

We further analysed the effect of nCRF stimulation on the temporal dynamics of orientation tuning. The *complexity* of the dynamics was measured by the orientation–time inseparability index, which was computed as the difference between the TOM and a reconstructed matrix that is completely separable (see Methods); a value of 0 indicates complete separability. Figure 7*A* shows the result of a cell at 1 × CRF stimulus size. The difference between the raw and the reconstructed matrix was relatively small, resulting in an inseparability index of 1.71. When the stimulus size increased to 4 × CRF (Fig. 7*B*), the inseparability index increased to 7.83. From our sample of 126 cells, the average inseparability index was 3.0 ± 0.3 at 1 × CRF, but the values were 4.4 ± 0.4 and 4.8 ± 0.4 at 2× and 4 × CRF, respectively, both of which were significantly larger than that at 1 × CRF ($P < 10^{-10}$ and $P < 10^{-12}$, paired *t* test) (Fig. 7*C*). This effect was found in all cortical layers (see Fig. 7 legend). Thus, nCRF stimulation increases the orientation–time inseparability, indicating that it affects the temporal dynamics of cortical orientation tuning. Taken together, all three analyses – temporal changes in tuning bandwidth and in preferred orientation and orientation–time inseparability – demonstrate that nCRF affects the temporal dynamics of orientation tuning.

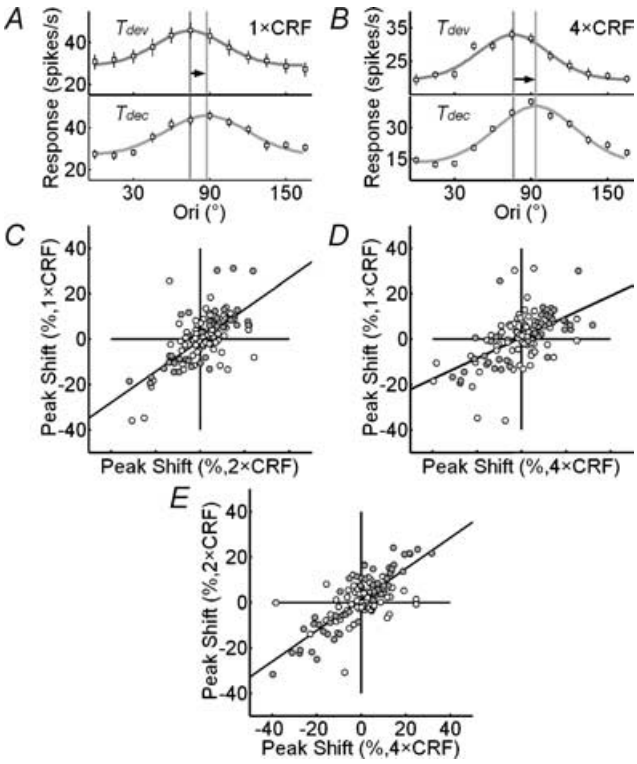

Figure 6. Dynamic changes in preferred orientation are enhanced by nCRF stimulation
A, orientation tuning curves of an example cell at T_{dev} and T_{dec} at 1 × CRF. Black and grey vertical lines, peak positions of the fitted curve (von Mises distribution) at T_{dev} and T_{dec}, respectively. The horizontal arrow indicates shift in the preferred orientation (13.1 deg). Error bar, ±S.E.M. *B*, tuning curves of the same cell at 4 × CRF. The shift in preferred orientation was 17.6°. *C–E*, comparison of shifts in preferred orientation between different sizes (*C*, at 1 × CRF *versus* that at 2 × CRF; *D*, at 1 × CRF *versus* that at 4 × CRF; *E*, at 2 × CRF *versus* that at 4 × CRF). The slopes of the robust regression (continuous lines) were 0.69, 0.46 and 0.68 for *C*, *D* and *E*, respectively, which were significantly different from zero (all $P < 10^{-10}$). Significant changes in preferred orientations over time at 1 × CRF (*C*), 2 × CRF (*E*) and 4 × CRF (*D*) are marked as filled points.

Discussion

In this study, we found that nCRF affects the temporal dynamics of orientation tuning, the decrease in

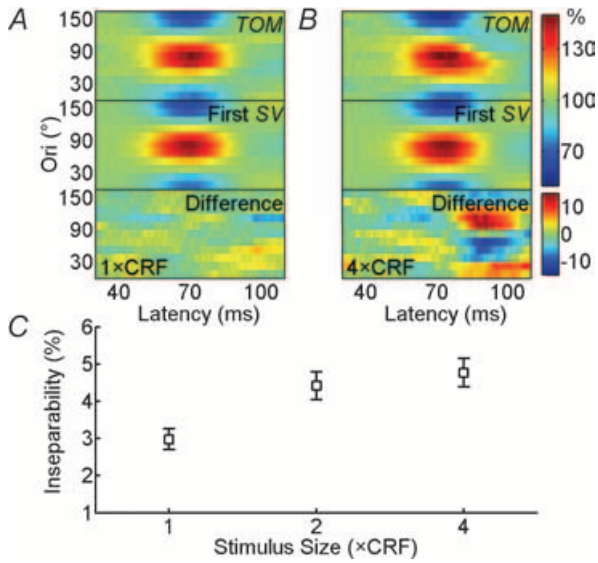

Figure 7. Stimulation of nCRF increases orientation–time inseparability of cortical neurones
A, TOM, its first singular vector reconstructed matrix, and the difference between these two matrixes for an example neurone at 1 × CRF (in unit of the percentage of the mean spike rate). Inseparability index was 1.71. *B*, same as *A*, but at 4 × CRF. The relatively high inseparability index (7.83) is largely caused by the tilt (upper-left to lower-right) of the TOM profile, which indicates a downward shift in the preferred orientation over time. *C*, inseparability index (see eqn (7) in Methods) as a function of stimulus size for 126 neurones. Error bar, ±S.E.M. The indices obtained with nCRF were significantly larger than those with CRF only, in all cortical layers; layer 2/3: 2.8 ± 0.5 for 1 × CRF *versus* 4.1 ± 0.7 ($P < 0.001$, paired *t* test) and 4.8 ± 0.7 ($P < 10^{-4}$) for 2× and 4 × CRF, respectively, $n = 44$; layer 4: 5.1 ± 1.2 *versus* 6.2 ± 1.5 ($P < 0.05$) and 6.3 ± 1.5 ($P < 0.05$), $n = 14$; layer 5/6: 3.6 ± 0.5 *versus* 5.3 ± 0.7 ($P < 0.001$) and 5.3 ± 0.7 ($P < 0.001$), $n = 33$. This effect was also found for both simple and complex cells; simple cells: 4.7 ± 0.6 for 1 × CRF *versus* 6.5 ± 0.9 ($P < 0.01$, paired *t* test) and 6.2 ± 0.8 ($P < 0.01$) for 2× and 4 × CRF, respectively, $n = 30$; complex cells: 2.4 ± 0.3 *versus* 3.8 ± 0.4 ($P < 10^{-8}$) and 4.3 ± 0.4 ($P < 10^{-10}$) $n = 96$. Cells with or without inhibitory nCRF also had a similar effect. Inhibitory: 2.7 ± 0.3 for 1 × CRF *versus* 4.1 ± 0.4% ($P < 10^{-5}$ paired *t* test) and 4.3 ± 0.4 ($P < 10^{-6}$) for 2× and 4 × CRF, respectively, $n = 68$; facilitatory: 3.2 ± 0.6 for 1 × CRF *versus* 4.2 ± 0.7 ($P < 0.001$) and 4.9 ± 0.7 ($P < 10^{-5}$) for 2× and 4 × CRF, $n = 42$; neither facilitatory nor inhibitory: 3.5 ± 1.0 for 1 × CRF *versus* 6.4 ± 1.6 ($P < 0.001$) and 6.5 ± 1.6 ($P < 0.001$) for 2× and 4 × CRF, $n = 16$.

bandwidth over time, and the shift in preferred orientation. In addition, nCRF causes an overall sharpening of orientation tuning, the magnitude of which increases with the area of stimulation.

Dynamics of orientation tuning

Many tuning properties in the visual cortex exhibit complex temporal dynamics. Selectivity for colour (Cottaris & De Valois, 1998), spatial frequency (Bredfeldt & Ringach, 2002), and stereoscopic depth (Menz & Freeman, 2003), are all found to be dynamic in V1. Dynamic changes in tuning have also been observed among the cells in the inferotemporal cortex that are selective for faces (Tovee, 1994; Sugase *et al.* 1999). These studies indicate that dynamic changes in neuronal response properties are prevalent in the cortex, which may have important functional implications in visual processing.

The temporal dynamics of orientation selectivity in V1 have been examined in several previous studies. Ringach *et al.* (1997*b*, 2003) measured the dynamics of orientation tuning in anaesthetized monkey using reverse correlation analysis, and reported that the tuning varied over time in some cells. However, other groups found no significant changes in the anaesthetized cat (Gillespie *et al.* 2001) or in the awake monkey (Mazer *et al.* 2002). Our studies provide possible explanations for the discrepancy. First, we found that the decrease in bandwidth (Fig. 5), the shift in preferred orientation (Fig. 6), and the orientation–time inseparability of TOM (Fig. 7), were all enhanced by nCRF stimulation. Thus experiments using stimuli confined within CRF (Gillespie *et al.* 2001) may not reveal the temporal dynamics of orientation tuning. Second, cortical neurones exhibit high response variability, which makes it difficult to demonstrate the significance of the changes using standard statistical analyses (Gillespie *et al.* 2001; Mazer *et al.* 2002). Here, we have demonstrated the non-randomness of the shift in preferred orientation over time using the correlation between the shifts measured at different sizes of the stimulation area (Fig. 6), which may be more sensitive for detecting the effect in the presence of high response variability. While our finding is basically consistent with that of Ringach *et al.* (1997*a*, 2003), we did not find significant difference in the orientation tuning dynamics across cortical layers. This may be due to the difference in the laminar structure between the cat and the monkey.

The temporal dynamics of orientation tuning may provide useful information on the underlying neuronal circuitry. The response of a cortical neurone is determined by a combination of feedforward, recurrent and feedback inputs. The latter two inputs, which may exhibit longer latencies (although feedback inputs to V1 have been found to have fast conduction axons (Nowak & Bullier, 1997; Girard *et al.* 2001) and terminate only in the supra- and infragranular layers of V1 (Angelucci & Bullier, 2003), so it may not contribute exclusively to the late responses in all cortical layers), are thought to play important roles in amplifying and modifying the response evoked by the feedforward input (Ben-Yishai *et al.* 1995; Somers *et al.* 1995; Adorjan *et al.* 1999). Since the recurrent and feedback inputs may differ from the feedforward input in their orientation tuning (Wang *et al.* 2000; Brown *et al.* 2003; Monier *et al.* 2003), their delayed arrival can cause systematic changes in the tuning of the neurone over a period of tens of milliseconds (Figs 5 and 6). Furthermore, the effects of nCRF stimulation on cortical responses are likely to be mediated by the recurrent or feedback inputs (Lamme & Roelfsema, 2000; Angelucci & Bullier, 2003). Enlarging the stimulation area to include nCRF may preferentially enhance the contributions of these inputs, thus amplifying the temporal changes in orientation tuning.

Effects of nCRF

In most of the previous studies investigating the effects of nCRF on orientation selectivity, stimulus orientation in CRF and nCRF were varied independently (Nelson & Frost, 1978; Gilbert & Wiesel, 1990; DeAngelis *et al.* 1994; Li & Li, 1994; Sillito *et al.* 1995; Sengpiel *et al.* 1997; Cavanaugh *et al.* 2002*b*; Muller *et al.* 2003), and these experiments have revealed the effects of nCRF stimulation on both the amplitude of the response and the peak position of orientation tuning within the CRF. In this study, we used uniform stimulation of CRF and nCRF, and found significant sharpening of the tuning curve by nCRF stimulation. It is important to note that increasing the stimulus size can sharpen the measured orientation tuning even within the CRF (Orban *et al.* 1984; Henrie & Shapley, 2001), and a bias in the estimated CRF size may affect the interpretation of the above finding. Most of previous studies used the area summation test to estimate the extent of CRF, but several studies have shown that spatial summation is not a fixed property but depends on the stimulus contrast (Kapadia *et al.* 1999; Sceniak *et al.* 1999). The estimated CRF size based on the occlusion test, on the other hand, was found to be relatively insensitive to contrast (Yao, 1998) and usually larger than that estimated with the summation test (Cavanaugh *et al.* 2002*a*). Thus the sharpening effect observed in the present study is unlikely to be due to the increased stimulation of the CRF (Henrie & Shapley, 2001). Furthermore, even if the occlusion test provided a somewhat conservative estimate of the CRF for some cells, it would be difficult to account for the finding that the sharpening effect induced by nCRF stimulation increased with stimulus size up to $4 \times$ CRF (which is comparable to the extent of nCRF found in other studies, e.g. Li & Li, 1994; Cavanaugh *et al.* 2002*a*). Finally, we found significant sharpening effect for cells

with inhibitory nCRF, which further indicates that the sharpening is mediated by a mechanism distinct from the excitatory CRF (e.g. recurrent or feedback inputs). Related to the present experiments using sinusoidal gratings, previous studies using bars have examined the influence of bar length on orientation selectivity (Henry *et al.* 1974*a*,*b*; Rose, 1977; Orban *et al.* 1979). The bandwidth of tuning was found to decrease with bar length within the CRF, but no further sharpening was found as the bar extends into the nCRF. This is different from the sharpening effect of nCRF we have found (Fig. 3*B*), probably because the CRF was estimated differently, and the bar stimuli activate smaller nCRF areas than the grating stimuli used here. The grating stimuli may excite a larger population of cells that are connected to the recorded cell, thus exerting a stronger influence.

Functionally, the modulatory effects of nCRF have been shown to reduce the coding redundancy in the visual cortex (Vinje & Gallant, 2000, 2002; Schwartz & Simoncelli, 2001). Our present findings demonstrate that nCRF stimulation also enhances cortical orientation selectivity and enriches its temporal dynamics. Since coding of stimulus orientation is an important function of the primary visual cortex, the above effects may further enhance the computational power of the cortical circuit in visual processing.

References

Adorjan P, Levitt JB, Lund JS & Obermayer K (1999). A model for the intracortical origin of orientation preference and tuning in macaque striate cortex. *Vis Neurosci* **16**, 303–318.

Akasaki T, Sato H, Yoshimura Y, Ozeki H & Shimegi S (2002). Suppressive effects of receptive field surround on neuronal activity in the cat primary visual cortex. *Neurosci Res* **43**, 207–220.

Allman J, Miezin F & McGuinness E (1985). Stimulus-specific responses from beyond the classical receptive field: neurophysiological mechanisms for local–global comparisons in visual neurons. *Annu Rev Neurosci* **8**, 407–430.

Anderson JS, Lampl I, Gillespie DC & Ferster D (2001). Membrane potential and conductance changes underlying length tuning of cells in cat primary visual cortex. *J Neurosci* **21**, 2104–2112.

Angelucci A & Bullier J (2003). Reaching beyond the classical receptive field of V1 neurons: horizontal or feedback axons? *J Physiol Paris* **97**, 141–154.

Ben-Yishai R, Bar-Or RL & Sompolinsky H (1995). Theory of orientation tuning in visual cortex. *Proc Natl Acad Sci U S A* **92**, 3844–3848.

Blakemore C & Tobin EA (1972). Lateral inhibition between orientation detectors in the cat's visual cortex. *Exp Brain Res* **15**, 439–440.

Bredfeldt CE & Ringach DL (2002). Dynamics of spatial frequency tuning in macaque V1. *J Neurosci* **22**, 1976–1984.

Bringuier V, Chavane F, Glaeser L & Fregnac Y (1999). Horizontal propagation of visual activity in the synaptic integration field of area 17 neurons. *Science* **283**, 695–699.

Brown HA, Allison JD, Samonds JM & Bonds AB (2003). Nonlocal origin of response suppression from stimulation outside the classic receptive field in area 17 of the cat. *Vis Neurosci* **20**, 85–96.

Cavanaugh JR, Bair W & Movshon JA (2002*a*). Nature and interaction of signals from the receptive field center and surround in macaque V1 neurons. *J Neurophysiol* **88**, 2530–2546.

Cavanaugh JR, Bair W & Movshon JA (2002*b*). Selectivity and spatial distribution of signals from the receptive field surround in macaque V1 neurons. *J Neurophysiol* **88**, 2547–2556.

Cottaris NP & De Valois RL (1998). Temporal dynamics of chromatic tuning in macaque primary visual cortex. *Nature* **395**, 896–900.

DeAngelis GC, Freeman RD & Ohzawa I (1994). Length and width tuning of neurons in the cat's primary visual cortex. *J Neurophysiol* **71**, 347–374.

Depireux DA, Simon JZ, Klein DJ & Shamma SA (2001). Spectro-temporal response field characterization with dynamic ripples in ferret primary auditory cortex. *J Neurophysiol* **85**, 1220–1234.

Dragoi V, Sharma J, Miller EK & Sur M (2002). Dynamics of neuronal sensitivity in visual cortex and local feature discrimination. *Nat Neurosci* **5**, 883–891.

Felsen G, Shen YS, Yao H, Spor G, Li C & Dan Y (2002). Dynamic modification of cortical orientation tuning mediated by recurrent connections. *Neuron* **36**, 945–954.

Fitzpatrick D (2000). Seeing beyond the receptive field in primary visual cortex. *Curr Opin Neurobiol* **10**, 438–443.

Gilbert CD (1977). Laminar differences in receptive field properties of cells in cat primary visual cortex. *J Physiol* **268**, 391–421.

Gilbert CD & Wiesel TN (1990). The influence of contextual stimuli on the orientation selectivity of cells in primary visual cortex of the cat. *Vision Res* **30**, 1689–1701.

Gillespie DC, Lampl I, Anderson JS & Ferster D (2001). Dynamics of the orientation-tuned membrane potential response in cat primary visual cortex. *Nat Neurosci* **4**, 1014–1019.

Girard P, Hupe JM & Bullier J (2001). Feedforward and feedback connections between areas V1 and V2 of the monkey have similar rapid conduction velocities. *J Neurophysiol* **85**, 1328–1331.

Golub GH & Van Loan CF (1996). *Matrix Computations*. Johns Hopkins University Press, Baltimore, MD, USA.

Henrie JA & Shapley RM (2001). The relatively small decline in orientation acuity as stimulus size decreases. *Vision Res* **41**, 1723–1733.

Henry GH, Bishop PO & Dreher B (1974*a*). Orientation, axis and direction as stimulus parameters for striate cells. *Vision Res* **14**, 767–777.

Henry GH, Dreher B & Bishop PO (1974*b*). Orientation specificity of cells in cat striate cortex. *J Neurophysiol* **37**, 1394–1409.

Jones HE, Grieve KL, Wang W & Sillito AM (2001). Surround suppression in primate V1. *J Neurophysiol* **86**, 2011–2028.

Jones HE, Wang W & Sillito AM (2002). Spatial organization and magnitude of orientation contrast interactions in primate V1. *J Neurophysiol* **88**, 2796–2808.

Kapadia MK, Westheimer G & Gilbert CD (1999). Dynamics of spatial summation in primary visual cortex of alert monkeys. *Proc Natl Acad Sci U S A* **96**, 12073–12078.

Knierim JJ & Van Essen DC (1992). Neuronal responses to static texture patterns in area V1 of the alert macaque monkey. *J Neurophysiol* **67**, 961–980.

Lamme VA (1995). The neurophysiology of figure-ground segregation in primary visual cortex. *J Neurosci* **15**, 1605–1615.

Lamme VA & Roelfsema PR (2000). The distinct modes of vision offered by feedforward and recurrent processing. *Trends Neurosci* **23**, 571–579.

Leventhal AG, Thompson KG, Liu D, Zhou Y & Ault SJ (1995). Concomitant sensitivity to orientation, direction, and color of cells in layers 2, 3, and 4 of monkey striate cortex. *J Neurosci* **15**, 1808–1818.

Levitt JB & Lund JS (1997). Contrast dependence of contextual effects in primate visual cortex. *Nature* **387**, 73–76.

Li CY & Li W (1994). Extensive integration field beyond the classical receptive field of cat's striate cortical neurons – classification and tuning properties. *Vision Res* **34**, 2337–2355.

Li CY, Xu XZ & Tigwell D (1995). A simple and comprehensive method for the construction, repair and recycling of single and double tungsten microelectrodes. *J Neurosci Methods* **57**, 217–220.

Lund JS, Henry GH, MacQueen CL & Harvey AR (1979). Anatomical organization of the primary visual cortex (area 17) of the cat. A comparison with area 17 of the macaque monkey. *J Comp Neurol* **184**, 599–618.

Maffei L & Fiorentini A (1976). The unresponsive regions of visual cortical receptive fields. *Vision Res* **16**, 1131–1139.

Manly BFJ (1997). *Randomization, Bootstrap and Monte Carlo Methods in Biology*. Chapman & Hall, London.

Mazer JA, Vinje WE, McDermott J, Schiller PH & Gallant JL (2002). Spatial frequency and orientation tuning dynamics in area V1. *Proc Natl Acad Sci U S A* **99**, 1645–1650.

Menz MD & Freeman RD (2003). Stereoscopic depth processing in the visual cortex: a coarse-to-fine mechanism. *Nat Neurosci* **6**, 59–65.

Monier C, Chavane F, Baudot P, Graham LJ & Fregnac Y (2003). Orientation and direction selectivity of synaptic inputs in visual cortical neurons: a diversity of combinations produces spike tuning. *Neuron* **37**, 663–680.

Muller JR, Metha AB, Krauskopf J & Lennie P (2003). Local signals from beyond the receptive fields of striate cortical neurons. *J Neurophysiol* **90**, 822–831.

Nelson JI & Frost BJ (1978). Orientation-selective inhibition from beyond the classic visual receptive field. *Brain Res* **139**, 359–365.

Nowak LG & Bullier J (1997). The timing of information transfer in the visual system. In *Extrastriate Visual Cortex in Primate*, ed. Rockland KS, Kaas JH & Peters A, pp. 205–241. Plenum Press, New York.

O'Leary J (1941). Structure of area striata of the cat. *J Comp Neurol* **75**, 131–164.

Orban GA (1984). *Neuronal Operations in the Visual Cortex*, vol. 11. Springer-Verlag, Berlin.

Orban GA, Kato H & Bishop PO (1979). End-zone region in receptive fields of hypercomplex and other striate neurons in the cat. *J Neurophysiol* **42**, 818–832.

Orban GA, Vandenbussche E & Vogels R (1984). Meridional variations and other properties suggesting that acuity and orientation discrimination rely on different neuronal mechanisms. *Ophthalmic Physiol Opt* **4**, 89–93.

Ozeki H, Sadakane O, Akasaki T, Naito T, Shimegi S & Sato H (2004). Relationship between excitation and inhibition underlying size tuning and contextual response modulation in the cat primary visual cortex. *J Neurosci* **24**, 1428–1438.

Pena JL & Konishi M (2001). Auditory spatial receptive fields created by multiplication. *Science* **292**, 249–252.

Polat U, Mizobe K, Pettet MW, Kasamatsu T & Norcia AM (1998). Collinear stimuli regulate visual responses depending on cell's contrast threshold. *Nature* **391**, 580–584.

Ringach DL, Hawken MJ & Shapley R (1997*a*). Dynamics of orientation tuning in macaque primary visual cortex. *Nature* **387**, 281–284.

Ringach DL, Hawken MJ & Shapley R (2003). Dynamics of orientation tuning in macaque V1: the role of global and tuned suppression. *J Neurophysiol* **90**, 342–352.

Ringach DL, Sapiro G & Shapley R (1997*b*). A subspace reverse-correlation technique for the study of visual neurons. *Vision Res* **37**, 2455–2464.

Rose D (1977). Responses of single units in cat visual cortex to moving bars of light as a function of bar length. *J Physiol* **271**, 1–23.

Rossi AF, Desimone R & Ungerleider LG (2001). Contextual modulation in primary visual cortex of macaques. *J Neurosci* **21**, 1698–1709.

Sceniak MP, Ringach DL, Hawken MJ & Shapley R (1999). Contrast's effect on spatial summation by macaque V1 neurons. *Nat Neurosci* **2**, 733–739.

Schwartz O & Simoncelli EP (2001). Natural signal statistics and sensory gain control. *Nat Neurosci* **4**, 819–825.

Sengpiel F, Baddeley RJ, Freeman TC, Harrad R & Blakemore C (1998). Different mechanisms underlie three inhibitory phenomena in cat area 17. *Vision Res* **38**, 2067–2080.

Sengpiel F, Sen A & Blakemore C (1997). Characteristics of surround inhibition in cat area 17. *Exp Brain Res* **116**, 216–228.

Sillito AM, Grieve KL, Jones HE, Cudeiro J & Davis J (1995). Visual cortical mechanisms detecting focal orientation discontinuities. *Nature* **378**, 492–496.

Skottun BC, De Valois RL, Grosof DH, Movshon JA, Albrecht DG & Bonds AB (1991). Classifying simple and complex cells on the basis of response modulation. *Vision Res* **31**, 1079–1086.

Somers DC, Nelson SB & Sur M (1995). An emergent model of orientation selectivity in cat visual cortical simple cells. *J Neurosci* **15**, 5448–5465.

Sugase Y, Yamane S, Ueno S & Kawano K (1999). Global and fine information coded by single neurons in the temporal visual cortex. *Nature* **400**, 869–873.

Swindale NV (1998). Orientation tuning curves: empirical description and estimation of parameters. *Biol Cybern* **78**, 45–56.

Tovee MJ (1994). Neuronal processing. How fast is the speed of thought? *Curr Biol* **4**, 1125–1127.

Vinje WE & Gallant JL (2000). Sparse coding and decorrelation in primary visual cortex during natural vision. *Science* **287**, 1273–1276.

Vinje WE & Gallant JL (2002). Natural stimulation of the nonclassical receptive field increases information transmission efficiency in V1. *J Neurosci* **22**, 2904–2915.

Walker GA, Ohzawa I & Freeman RD (1999). Asymmetric suppression outside the classical receptive field of the visual cortex. *J Neurosci* **19**, 10536–10553.

Wang C, Waleszczyk WJ, Burke W & Dreher B (2000). Modulatory influence of feedback projections from area 21a on neuronal activities in striate cortex of the cat. *Cereb Cortex* **10**, 1217–1232.

Worgotter F & Eysel UT (1987). Quantitative determination of orientational and directional components in the response of visual cortical cells to moving stimuli. *Biol Cybern* **57**, 349–355.

Yao HS (1998). Functional Architecture and Structure and Function of the Integration Field of Cat's Primary Visual Cortical Neurons. Thesis, Shanghai Institute of Physiology, Chinese Academy of Sciences, Shanghai, China.

Yao H & Li CY (2002). Clustered organization of neurons with similar extra-receptive field properties in the primary visual cortex. *Neuron* **35**, 547–553.

Yao H, Shen Y & Dan Y (2004). Intracortical mechanism of stimulus-timing-dependent plasticity in visual cortical orientation tuning. *Proc Natl Acad Sci U S A* **101**, 5081–5086.

Acknowledgements

We gratefully acknowledge the expert technical assistance of Ms. Xing-Zhen Xu. We also thank two anonymous reviewers for constructive comments and suggestions. This research was supported by grants from the Major State Basic Research Program (G2000077804), the Natural Science Foundation of China (90208006 and 30028004), the Program of Brain and Mind of CAS (KJCX1-07), the laboratory of Visual Information Processing of CAS, and the Laboratory of Mental Health of CAS.